Journal of Engineering Mathematics, Vol. 7, No. 4, October 1973
Noordhoff International Publishing–Leyden
Printed in The Netherlands



# Two-dimensional buoyant jet in a current

H. O. ANWAR

*Hydraulics Research Station, Wallingford, England*

(Received August 4, 1972 and in revised form February 12, 1973)

SUMMARY

When an effluent is discharged into a current at or near the bed, it may be advantageous to have the effluent flowing along the bed for some distance, thickening en route, so that it will have become diluted sufficiently before it reaches the surface. This can be achieved provided the effluent is discharged from a narrow long slot into the ambient current; the effluent plume then flows near the bed due to the pressure drop on the lee side of the emerging effluent.

To confirm that this type of effluent flow could exist, laboratory experiments were conducted in which warm water at about 76° C was discharged vertically upwards from a slot 1 cm wide into an ambient current at a temperature of about 12° C. It was observed that the discharged effluent rose a short distance above the slot, due to its initial momentum, and then re-attached itself to the rigid floor, continuing along the floor as it slowly thickened. The temperature and its fluctuation, the velocity and the thickness of the layer, were measured for various ratio of the ambient velocity to the jet velocity and densimetric Froude numbers at the slot. It was found that flow in the layer at a certain distance from the slot is dynamically similar, and that the measured data can be described by non-dimensional similarity functions in the density and velocity field. It was also shown, both theoretically and experimentally, that the depth and the dilution factor, based on the maximum temperature of the under-flowing layer, increases linearly with down-stream distance from the slot.

It was further found that the coefficient of skin friction depends on Richardson number and that the coefficient remains constant for a given flow condition.

## Notation

$C_1$, $C_2$ constant coefficients equation (2.12).
$C_f$ coefficient of skin friction.
$F_0$ densimetric Froude number equation (4.9).
$F_x$, $F_y$ components of the buoyancy force in $x$ and $y$ direction.
$f_1(\eta)$, $f_2(\eta)$, $g_1(\eta)$, $g_2(\eta)$, $g_{12}(\eta)$ universal functions equation (2.4).
$g$ acceleration due to gravity.
$I_1$, $I_2$ integrals of function $f_1(\eta)$ and $f_2(\eta)$ equation (2.15).
$h$ characteristic thickness of the underflowing layer.
$h_0$ depth of the warm layer at section A–A (Fig. 1).
$H$ depth of the ambient current.
$n$ index associated with raw data.
$N$ total number of digitized data.
$p$ pressure.
$R$ ratio of the ambient velocity to the jet velocity.
$R_e$ Reynolds number based at the slot.
$R_i$ Richardson number equation (2.12).
$T$ local arithmetic mean value of temperature.
$T_0$ temperature of the jet at slot exit.
$T_a$ temperature of the ambient current.
$T_m$ maximum temperature at each section.
$t_n$ instantaneous point temperature.
$t$ time.
$\overline{(t'^2)}^{\frac{1}{2}}$ root-mean-square of temperature.
$U$ local mean velocity in the mean flow direction.
$U_a$ average mean velocity of the ambient current (see Fig. 1).

$U_0$ jet velocity at the slot exit.
$U_*$ shear velocity.
$V$ local mean velocity in the vertical direction.
$\bar{u}, \bar{v}$ velocity fluctuation of $U$ and $V$ component respectively.
$w$ slot width.
$X_0$ non-dimensional distance from the virtual origin.
$x, y$ system of co-ordinates (Fig. 1).
$\delta$ relevant length scale at which the temperature excess is half of its maximum value.
$\eta$ non-dimensional transverse distance.
$\theta$ angle of inclination of the rigid boundary.
$\lambda$ ratio between the length scale $\delta$ and the characteristic thickness $h$.
$\nu$ kinematic viscosity.
$\rho$ local mass density.
$\rho_0$ mass density at slot exit.
$\rho_a$ mass density of the ambient current.
$\Delta\rho_0$ mass density excess at the slot exit.
$\Delta\rho_m$ maximum of mass density excess at each section.
$\tau_0$ shear stress at rigid boundary.
$\varphi_1, \varphi_2, \psi_1, \psi_2$ universal functions equations (4.5, 4.6, 4.7, 4.8).

## 1. Introduction

There are many ways of discharging an effluent such as sewage or warm water from the cooling system of a power station into a river or into a tidal current. The effluent can be discharged either vertically upwards [1] or horizontally [2], [3] through a plain single open shaft, [1] or through a diffuser port in such way that the rising columns from the holes do not interfere with each other [4], [5]. The outfall may also be such that the effluent is discharged from a single slot (about 100 m long) into the current. In this last case the discharged fluid will flow near the bed for a considerable distance, so that when it eventually reaches the free surface it will be diluted sufficiently for there to be no significant pollution hazard. So far as the writer is aware, there are few outfalls of a slot type in existence, and it is hoped that this paper, describing as it does the behaviour of a buoyant jet discharged from a long slot into a cross flow, will be considered by design engineers as offering an alternative approach to the design of submarine outfalls.

Experimentally warm water at about 76°C was discharged vertically upwards into an ambient current at about 12°C. The width of the slot was 1 cm and its length was equal to the width of the flume. The mean velocity, mean temperature and temperature fluctuation were measured across the layer at various downstream distances from the slot, and the thickness of the layer was determined from the measured temperature profiles.

It was observed that the buoyant jet reattaches itself to the floor at a certain downstream distance from the slot, and that this distance depends on the ratio of the ambient velocity to the jet velocity. Theoretically it was assumed that the flow of the reattaching buoyant jet is self-similar, but such similarity is violated at the point of reattachment. It was also assumed that downstream from the reattachment point the flow of the warm layer, as it entrains the ambient fluid, recovers over a certain length, beyond which for the theoretical purposes it is assumed that the flow patterns are again self-similar in successive sections. The results of the theoretical approach were compared with those obtained experimentally.

## 2. Theory

It will be assumed in what follows that the motion of the warm underflowing layer is steady, and thus that the tip of the layer is sufficiently far from the slot.

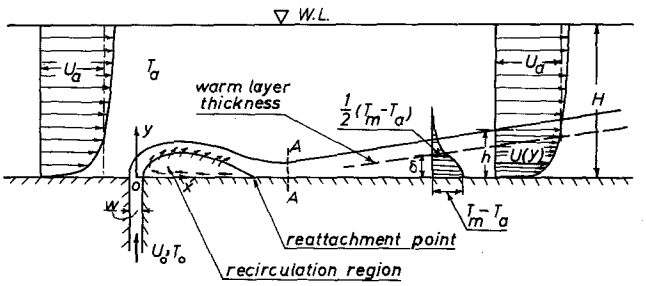


Figure 1. Definition of terms for two-dimensional buoyant jet in a current.

Let the Boussinesque approximation be made, namely that the density difference between the ambient current and the warm layer can be neglected except where multiplied by $g$, the acceleration due to gravity. Thus the equations of motion for a turbulent, incompressible flow of the underflowing layer may be written as follows, using the system of co-ordinates shown in Fig. 1.

*Momentum*

$$U\frac{\partial U}{\partial x}+V\frac{\partial U}{\partial y}=F_x-\frac{1}{\rho_a}\frac{\partial p}{\partial x}+\frac{\partial}{\partial x}\left(\nu\frac{\partial U}{\partial x}-\overline{u^2}\right)+\frac{\partial}{\partial y}\left(\nu\frac{\partial U}{\partial y}-\overline{uv}\right) \tag{2.1}$$

$$U\frac{\partial V}{\partial x}+V\frac{\partial V}{\partial y}=F_y-\frac{1}{\rho_a}\frac{\partial p}{\partial y}+\frac{\partial}{\partial x}\left(\nu\frac{\partial V}{\partial x}-\overline{uv}\right)+\frac{\partial}{\partial y}\left(\nu\frac{\partial V}{\partial y}-\overline{v^2}\right) \tag{2.2}$$

*Continuity*

$$\frac{\partial U}{\partial x}+\frac{\partial V}{\partial y}=0 \tag{2.3}$$

In the above equations $x$, $y$ are the systems of co-ordinates shown in Fig. 1, $U$ and $V$ are the respective local mean velocities with their velocity fluctuation $\bar{u}$ and $\bar{v}$, $p$ is the pressure, $F_x$ and $F_y$ are the components of the buoyancy force in $x$ and $y$-direction respectively, and $\rho_a$ is the mass density of the ambient current. In order to proceed with the above equations it will be assumed, as usually is the case in rivers or estuaries, where an outfall is situated, that the flow of the ambient current is fully turbulent. By this, is meant that the turbulent boundary layer has reached the free surface upstream of the slot. Hence the mean velocity, $U$, of the ambient current depends on $y$ alone; furthermore, the turbulent structure near the solid boundary is wholly determined by a "friction velocity" $U_*=(\tau_0/\rho_a)^{\frac{1}{2}}$ where $\tau_0$ is the constant shear stress at the solid boundary. Experiment showed that the buoyant jet reattached itself to the solid boundary at a certain distance downstream from the slot (see Section 4). Here it is assumed that the flow in the reattaching buoyant jet is similar to that of a two-dimensional reattaching momentum jet in a stagnant ambient fluid as investigated by Sawyer [6], [7]; he showed that the flow of the curved jet is very close to that of a plane jet. In other words the flow in the reattaching momentum jet is self-similar. The assumption of self-similarity for a reattaching buoyant jet in an ambient current may be questioned, but in view of the lack of detailed measurements it is reasonable to accept this assumption.

Now it will be assumed that the self-similarity of the flow of the reattaching buoyant jet is violated in the region near the reattachment point, and that the turbulent structure of the underflowing layer is perturbed in the sense that the flow along a certain distance downstream from the reattachment point cannot be considered to be similar to the flow in the boundary-layer flow. This means that the change of the tangential Reynolds stress is not negligible near the solid boundary. In other words the friction velocity $U_*$ cannot be accepted, as is the case in the boundary-layer flow, as a scaling velocity. But it will be assumed that the flow of the underflowing layer, downstream of the reattachment point (see Fig. 1), takes a certain length

to recover to the type of motion in a boundary-layer flow, i.e. the flow patterns are dynamically similar in successive sections downstream from the recovery length. This assumption has been confirmed experimentally by measurement of the mean velocity and also by measurement of the mean temperature and its fluctuation, but such measurements may not constitute a complete test for the validity of the similitude of the considered flow. However, with this assumption it is possible to look for non-dimensional functions like $f_1(\eta)$ for the velocity and $f_2(\eta)$ for the density distribution in which $\eta$ is the transverse distance made dimensionless with an $x$-dependent characteristic dimension. As the flow of the warm layer approaches a boundary layer flow the friction velocity $U_*$ can be taken as a velocity scale; unfortunately no measurement was carried out to determine $U_*$; on the other hand it was found experimentally that beyond the recovery length, the average mean velocity, $U_a$, (see Fig. 1) of the ambient current over the flow section, and the density differences between the density of the ambient current and the maximum density in the warm layer, and also the thickness, $h$, of the warm layer are the suitable characteristic quantities. Hence the following functions may be defined.

$$\left.\begin{aligned} &U = U_a f_1(\eta), \quad \Delta\rho = \Delta\rho_m f_2(\eta), \quad \overline{u^2} = U_a^2 g_1(\eta) \\ &\overline{v^2} = U_a^2 g_2(\eta), \quad \overline{uv} = U_a^2 g_{12}(\eta) \end{aligned}\right\} \tag{2.4}$$

in which $\eta = y/h$ $\Delta\rho = \rho_a - \rho$, with $\rho$ the mass density of the warm layer and $\Delta\rho_m$ is the maximum of the density differences at various sections downstream from the slot. The non-dimensional functions (2.4) and the definition of $\eta$ can usually be determined experimentally, but this, as mentioned before, does not mean that the existence of such functions obtained experimentally thus yields an analytical similitude or *vice-versa.*

Equation (2.2) can be written in the following form by making use of expression (2.4) and of the continuity equation (2.3).

$$-\frac{1}{\rho_a}\frac{\partial p}{\partial y} - \frac{U_a^2}{h} g_2'(\eta) - g\frac{\Delta\rho(x, y)}{\rho_a} = 0 \tag{2.5}$$

It is to be noted that equation (2.5) was derived on the assumption that the terms $\partial^2 h/\partial x^2$, $(\partial h/\partial x)^2$ and also the variation of the average mean velocity, $U_a$, (scale velocity) at various downstream sections beyond the recovery length, are negligibly small. This in fact was confirmed experimentally as described later. The third term on the left hand side of equation (2.5) represents the vertical component of the buoyancy force and the prime in the equation refers to the differentiation with respect to $\eta$. The above equation will now be integrated to define the pressure, $p$, i.e.

$$p(x, y) + \rho_a U_a^2 g_2(\eta) = -g\int_h^y \Delta\rho(x, y)dy + P_a(x). \tag{2.6}$$

The lower limit of the integral at the right-hand side of equation (2.6) is the height at which the left-hand side of the above equation is equal to $P_a(x)$, which is a function of $x$ alone, hence an expression for $P_a(x)$ can be given in the following form

$$P_a(x) = -g\rho_a(h - H) \tag{2.7}$$

in which $h$ and the total depth, $H$, (see Fig. 1) are a function of $x$ only. By substituting equation (2.7) into equation (2.6) the pressure term, $p$, can be expressed in the following form.

$$p(x, y) = -\rho_a U_a^2 g_2(\eta) - g\int_h^y \Delta\rho(x, y)dy - g\rho_a(h - H). \tag{2.8}$$

For the derivation of the above equation the assumption was made that there is no acceleration in the entire flow, hence a term representing a dynamic pressure due to the fluid acceleration is not included in the above equation. Equation (2.8) will now be differentiated with respect to $x$ in order to determine the term for the pressure gradient in equation (2.1), hence:

$$\frac{\partial p(x, y)}{\partial x} = -g\int_h^y \frac{\partial \Delta\rho(x, y)}{\partial x} dy + g(\Delta\rho(x, y) - \rho_a)\frac{\partial h}{\partial x} + g\rho_a\frac{\partial H}{\partial x}. \tag{2.9}$$

The term for $\Delta\rho$ given in expressions (2.4) is now substituted into equation (2.9) and the obtained equation together with expressions (2.4) are substituted into equation (2.1). This equation, with suitable re-arrangement and making use of the continuity equation (2.3), is as follows.

$$-\frac{\partial h}{\partial x} f_1'(\eta) \int f_1(\eta) d\eta + \frac{g \dfrac{\Delta\rho_m}{\rho_a} h}{U_a^2} f_2(\eta) \sin\theta - \frac{\partial h}{\partial x} \eta g_1'(\eta)$$

$$- \frac{h^2}{U_a^2} \frac{\partial \left( g \dfrac{\Delta\rho_m}{\rho_a} \right)}{\partial x} \int f_2(\eta) d\eta + \frac{gh \dfrac{\Delta\rho_m}{\rho_a}}{U_a^2} \frac{\partial h}{\partial x} \left[ (\eta+1) f_2(\eta) - \int f_2(\eta) d\eta \right] + g_{12}'(\eta)$$

$$- \frac{gh}{U_a^2} \left( \frac{\partial h}{\partial x} - \frac{\partial H}{\partial x} \right) = \frac{\nu}{U_a h} f_1''(\eta) . \tag{2.10}$$

The second term on the left-hand side of the above equation represents $F_x$, in which $\theta$ is the angle of inclination of the solid boundary (see Fig. 1). It is a known fact that in a turbulent flow the viscous stress is small compared to the turbulent shear stress, except very close to a rigid boundary. Hence, it is reasonable to assume that the term on the right-hand side of equation (2.10) is negligible. Now it can be stated that a self-similar flow can only exist when the coefficient of the non-dimensional function of the differential equation of motion is either zero or a non-zero constant. This, of course, cannot apply to equation (2.10), because of the term

$$\frac{gh}{U_a^2} \left( \frac{\partial h}{\partial x} - \frac{\partial H}{\partial x} \right),$$

in which $\partial H/\partial x$, the slope of the water surface, is negligibly small, at least for the cases, that have been studied by the author; but the term $(gh/U_a^2) \cdot (\partial h/\partial x)$ may not be negligible (*i.e.* where $U_a$ is small and $\partial h/\partial x$ is large). This means that an "analytical similarity", as it will be termed here, cannot be obtained when the term $(gh/U_a^2) \cdot (\partial h/\partial x)$ is large compared to the other term of the equation of motion. In other words, an analytical similarity can only be obtained when the term

$$\frac{gh}{U_a^2} \left( \frac{\partial h}{\partial x} - \frac{\partial H}{\partial x} \right) \approx 0 .$$

This, in fact, represents the condition in the boundary-layer flow without pressure gradient, and does not apply to the case considered here, but from the results of the experimental study (see Section 4) it seems that, for the considered cases, the absence of an analytical similarity does not rule out the existence of an experimental similarity. However, in order to obtain an approximate analytical similarity it will be assumed that the term $(gh/U_a^2) \cdot (\partial h/\partial x)$ is negligibly small compared to the other terms in equation (2.10). Hence the solution of equation (2.10) requires that the coefficient of the non-dimensional functions be either zero or a non-zero constant. Thus the non-repetitive coefficients are:

$$\frac{dh}{dx}, \quad \frac{d\left( g \dfrac{\Delta\rho_m}{\rho_a} \right)}{dx} \frac{h^2}{U_a^2}, \quad \frac{g \dfrac{\Delta\rho_m}{\rho_a} h}{U_a^2} \frac{dh}{dx} . \tag{2.11}$$

The above coefficients were derived by considering the angle $\theta$ to be small, hence the coefficient containing the term $\sin\theta$ is negligible. Each of the coefficients in equation (2.11) must be equal to a constant, thus

$$h = C_1 x , \quad g \frac{\Delta\rho_m}{\rho_a} = C_2 x^{-1} \quad \text{and} \quad \frac{g \dfrac{\Delta\rho_m}{\rho_a} h}{U_a^2} = C_3 . \tag{2.12}$$

Expression (2.12) shows that the depth of the layer $h$ varies linearly with $x$ and the maximum density difference $\Delta\rho_m$ varies with the reciprocal of the downstream distance $x^*$, so that the sectional Richardson number $R_i = g(\Delta\rho_m/\rho_a)h/U_a^2$ remains constant. The constants $C_1$ and $C_2$ will be defined later.

At this stage it may be useful to obtain information about the friction (resistance) coefficient.

Equation (2.1) can be written in the following form assuming that the scale velocity $U_a$ is constant at various downstream sections from the slot and also that the term $\partial\overline{u^2}/\partial x$ is small compared with the term $\partial\overline{uv}/\partial y$, hence

$$U\frac{\partial U}{\partial x} + V\frac{\partial U}{\partial y} = -\frac{1}{\rho_a}\frac{\partial p}{\partial x} - \frac{\partial\overline{uv}}{\partial y} \tag{2.13}$$

in which, as before, it has been assumed that the viscous stress and the angle $\theta$ are small. Equation (2.13) will be integrated with respect to $y$ to give the following equation by making use of equation (2.3)

$$\frac{\tau_0}{\rho_a} = \frac{1}{\rho_a}\int_0^h \frac{\partial p}{\partial x}\,dy + \int_0^h \frac{\partial U^2}{\partial x}\,dy - U_a\int_0^h \frac{\partial U}{\partial x}\,dy \tag{2.14}$$

where $\tau_0$ designates the wall shear stress, subject to the condition that $\tau_0 = 0$ at the height $h$. By substituting equation (2.9) into the above equation and making use of the expressions given in equation (2.4), the following expression for the wall shear stress can be obtained.

$$\frac{\tau_0}{\rho_a} = -h^2\frac{\partial\left(g\dfrac{\Delta\rho_m}{\rho_a}\right)}{\partial x}\int_0^1 I_1\,d\eta + gh\frac{\partial h}{\partial x}\left[\frac{\Delta\rho_m}{\rho_a}\left(\int_0^1 I_2\,d\eta + \int_0^1 f_2\,d\eta\right) - 1\right]$$
$$-U_a^2\frac{\partial h}{\partial x}\left[\eta f_1^2\Big|_0^1 - \eta f_1\Big|_0^1 - \int_0^1 f_1^2\,d\eta + \int_0^1 f_1\,d\eta\right] \tag{2.15}$$

where $I_1 = \int_0 f_2\,d\eta$ and $I_2 = [\eta f_2 - \int_0 f_2\,d\eta]$.

The above equation will take the following form in term of the coefficient of skin friction:

$$\frac{\tau_0}{\rho_a U_a^2} = \tfrac{1}{2}C_f = -\frac{h}{U_a^2}\frac{\partial\left(g\dfrac{\Delta\rho_m}{\rho_a}\right)}{\partial x}\int_0^1 I_1\,d\eta + \frac{gh}{U_a^2}\frac{dh}{dx}\left[\frac{\Delta\rho_m}{\rho_a}\left(\int_0^1 I_2\,d\eta + \int_0^1 f_2\,d\eta\right) - 1\right] +$$
$$-\frac{\partial h}{\partial x}\left[\eta f_1^2\Big|_0^1 - \eta f_1\Big|_0^1 - \int_0^1 f_1^2\,d\eta + \int_0^1 f_1\,d\eta\right]. \tag{2.16}$$

The term $(gh/U_0^2)\cdot(\partial h/\partial x)$ as discussed before, is negligibly small, and so is the ratio $\Delta\rho_m/\rho_a$, hence it is reasonable to assume that the second term on the right-hand side of equation (2.16) is small compared with the other terms of the equation. The equation may therefore be written as follows.

$$\frac{\tau_0}{\rho_a U_a^2} = \tfrac{1}{2}C_f = -\frac{h^2}{U_a^2}\frac{\partial\left(g\dfrac{\Delta\rho_m}{\rho_a}\right)}{\partial x}\int_0^1 I_1\,d\eta$$
$$-\frac{\partial h}{\partial x}\left[\eta f_1^2\Big|_0^1 - \eta f_1\Big|_0^1 - \int_0^1 f_1^2\,d\eta + \int_0^1 f_1\,d\eta\right]. \tag{2.17}$$

It is now permissible to substitute expression (2.12) into equation (2.16), which then, with suitable rearrangement, can be written in the following form:

$$\tfrac{1}{2}C_f = C_1 R_i\int_0^1 I_1\,d\eta - C_1\left[\eta f_1^2\Big|_0^1 - \eta f_1\Big|_0^1 - \int_0^1 f_1^2\,d\eta + \int_0^1 f_1\,d\eta\right]. \tag{2.18}$$

* The value of the exponent obtained for a line source in wind tunnel experiments is $-0.9$ and for field data varies between $-0.9$ and $-1$ [8] [9] [10]. The fair agreement between these results and the calculation suggests that the term $(gh/U_a^2)\cdot(\partial h/\partial x)$ was in fact negligibly small for the considered cases.

Equation (2.18) shows that the value of $R_i \int_0^1 I_1 \, d\eta$ must be larger than or equal to the value in the bracket on the right-hand side of equation (2.18), otherwise the shear stress is negative, which is not acceptable. However, the value of $C_f$ will be discussed later when the values of the integrals and $C_1$ are determined from the experimental results.

## 3. Experiments

The experiments were conducted in a transparent-walled flume 10 m long, 0.6 m wide, and 1.2 m high. The transition from the entrance section into the flume was formed with two parabolic walls, a screen and a honeycomb 1 m long and $6 \times 6$ cm cross section and 1.5 mm thick. The honeycomb was placed 2.20 m upstream from the slot. This arrangement provided a smooth and uniform flow as confirmed by the measured velocity profiles at various sections in the flume. The exit of the flume was provided with a series of inclined rods to control flow depth. Water at about 76° C was supplied from a storage tank with a capacity of 28 $m^3$. The warm water discharge was registered by a variable orifice meter and the ambient current was circulated by a 0.23 $m^3/s$ pump. The water from the flume flowed into a large reservoir beneath, to which cold water was added continuously during the experiment.

After an hour the experiment had to be stopped to correct the ambient temperature. A rectangular duct 0.6 m long, 1 cm wide and 15 cm deep was fitted flush to the false floor, which had a smooth surface. The rectangular duct was positioned at about 2.5 m downstream from the entrance to the flume. In order to ensure that the flow from the rectangular duct was of a two-dimensional form, it was found necessary to place two meshes of different size in the transition section; this was positioned between the duct and the 10 cm diameter supply pipe. The longitudinal velocity was then measured across the plane of symmetry parallel to the length of the duct.

The velocity measurements indicated that the maximum velocity at the slot was constant across the slot length to 1% for the range of $U_0$, between 15 and 75 cm/s. The temperature and its fluctuation were measured with a thermistor of type, $F$, obtained from Standard Telephone & Cables Ltd. The time constant of thermistor, which is that taken to respond to $(e-1)/e \simeq 0.63$ $(e=2.178)$ of a steep change in temperature, was measured and found to be about $\frac{1}{4}$ second when it was immersed in well agitated water. The thermistor was connected to a data-logger. The data-logger was in turn connected to a punched paper tape output, which recorded 10 samples every second. The time for taking samples at each point of the layer was about 100 seconds. The variation of the mean temperature and its fluctuation with the duration of the sampling period can be seen in Fig. 2. This shows that the measured data remained almost unchanged when the sampling time exceeded 90 seconds. The r.m.s. and the mean values of

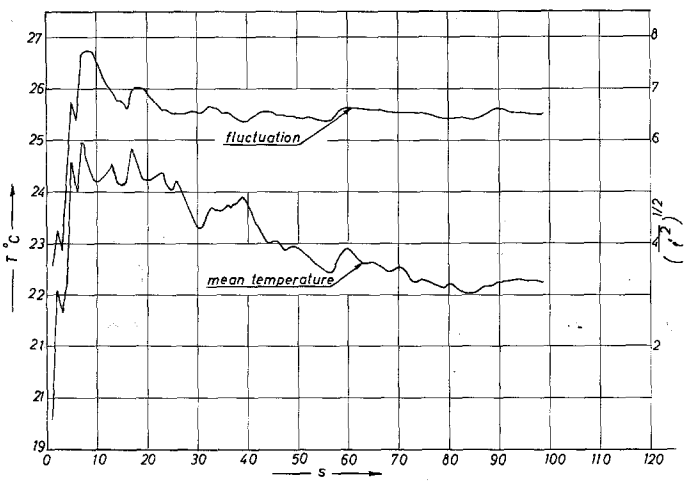


Figure 2. Variation of mean temperature and root-mean-square value of temperature with the duration of sampling.

the temperature were evaluated from the punched tape, using a digital computer to calculate the arithmetical mean value according to the following expression:

$$T = \frac{1}{N}\sum_{n=1}^{N} t_n, \qquad (\overline{t'^2})^{\frac{1}{2}} = \left[\frac{1}{N}\sum_{n=1}^{N}(t_n - T)^2\right]^{\frac{1}{2}}. \tag{3.1}$$

Velocity at points was measured with a current meter of 1 cm propeller diameter.

The above mentioned measurements were carried out along the centre line of the flume, assuming that the effect of secondary flow is negligible on this line.

## 4. Experimental results

It was observed that the warm water discharged from the slot after a short rise, due to its initial momentum, re-attached itself to the false floor and then behaved similar to that investigated by Sawyer [6] [7]. The buoyant jet was curved toward the floor causing a pressure difference across the jet (see Fig. 3). On impinging against the floor the jet divided and a portion of it flowed into the cavity. The fluid flowing into the cavity was, in turn, entrained by the inner edge of the jet, as shown in Fig. 1. The length and the height of the cavity was found to depend on the velocity ratio $R = U_a/U_0$.

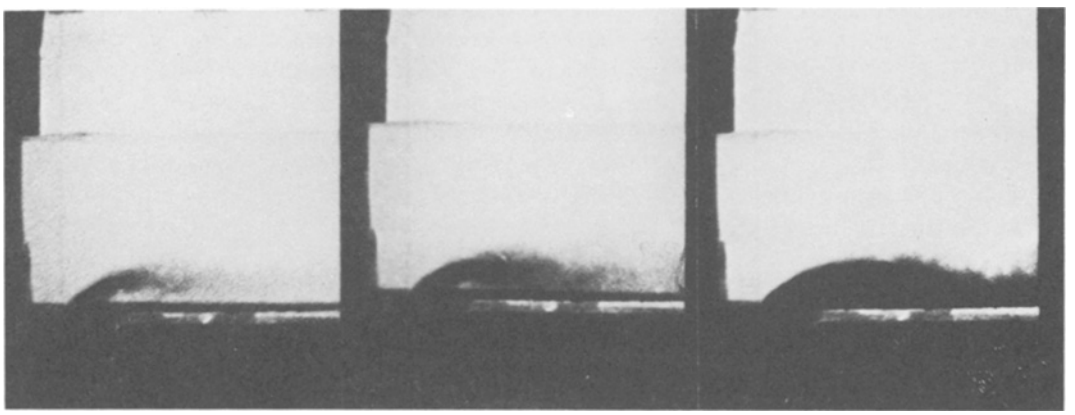

Figure 3. Reattachment of a two-dimensional buoyant jet to the floor.

### 4.1 *Temperature profile*

The mean value of the temperature was obtained according to the first expression of equation (3.1) and the temperature measurements were carried out across the sections at various downstream distances $x$. The results of the measurements, when $R$ varies between 0.5 and 1.5, are shown in dimensionless form in Fig. 4. In this Figure, $w$ is the slot width and $\delta$ is a relevant

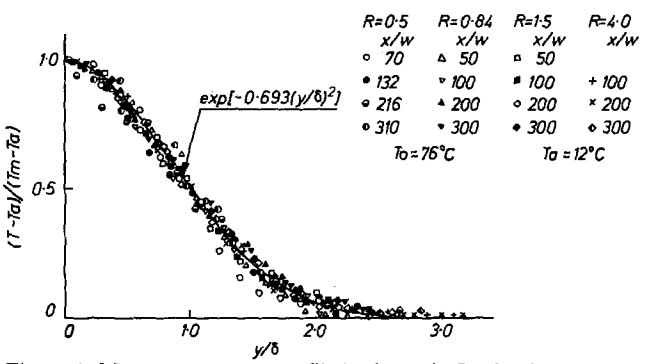


Figure 4. Mean temperature profile in the underflowing layer.

length scale, given by $y=\delta$ where the temperature excess $(T-T_a)$ is half of its maximum value which occurs very close to the false floor, $T$ is the mean temperature at any point $y$ with its maximum value $T_m$ (temperature scale) when $y\simeq 0$. These profiles were found to be geometrically similar and a good empirical fit to them can be given by the following expression:

$$\frac{T-T_a}{T_m-T_a}=\exp\left[-0.693\left(\frac{y}{\delta}\right)^2\right]. \tag{4.1}$$

Fig. 5 shows the turbulent intensity of temperature fluctuations plotted non-dimensionally. The measured points in Fig. 5 are scattered, due to the fact that the thermistor was not sensitive enough for the temperature fluctuation. This means that if there were fluctuations in the high frequencies of temperatures, as probably was the case for $R=1.5$, then the thermistor did not respond to them. Fig. 4 shows that, within the experimental scatter, the flow is dynamically similar when $x/w$ is larger than 100. Fig. 5, on the other hand, supports the similarity assumption when $x/w=200$.

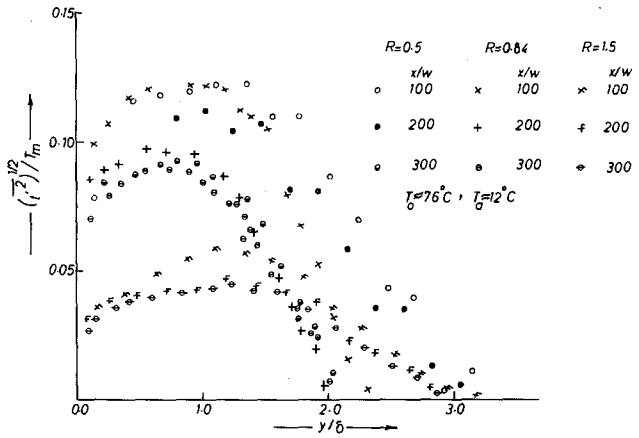


Figure 5. Profiles of turbulent intensity of temperature fluctuation.

The results of the velocity measurements for various sections downstream from the slot are shown in Figs 6 and 7. Figure 6 shows the mean velocity profiles in the recovery zone, the existence of which was assumed in the theoretical model. The measured profiles approach a universal function (Fig. 7) when the non-dimensional longitudinal distance $x/w$ is larger than 200. In other words, the profiles of the velocity and of the turbulent intensity of temperature fluctuations indicate that the length of recovery to a self similar flow is about 200 times the slot width. On the other hand, this length was about 100 times the slot width for the mean temperature profiles. This may be interpreted by saying that the velocity and the temperature fluctuation are more sensitive to perturbation than the mean temperature. However, an empirical fitted

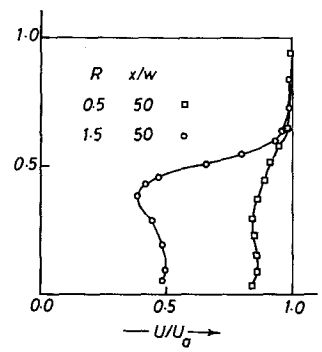


Figure 6. Mean velocity profiles in the recovery zone.

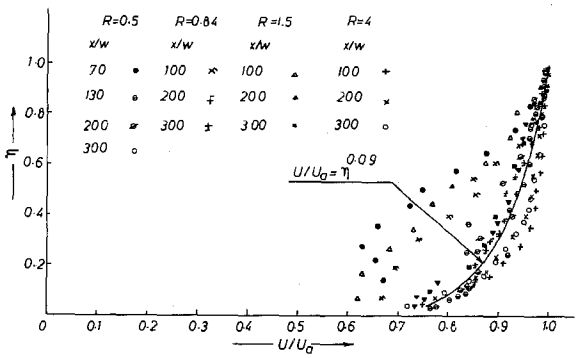


Figure 7. Mean velocity profiles in the underflowing layer.

curve to the velocity profiles can be given by the following expression:

$$\frac{U}{U_a} = \left(\frac{y}{h}\right)^{0.09} \tag{4.2}$$

In the above equation, $h$ is the depth at which the velocity ratio $U/U_a \simeq 0.98$. This was determined from the measured velocity profiles. The solid line drawn between $\eta = 0.05$ and $\eta = 1$ represents the above equation. The results obtained for $R = 4$ indicate a variation of the exponent in equation (4.2). This variation could not be determined experimentally, because the highest value of $R$, which could be obtained in the experimental set-up, was 4. However, equation (4.2) will be used to evaluate the integrals in equation (2.18). It can be seen that a small variation of the exponent in equation (4.2) will change the value of the integral slightly.

It has previously been shown that when the flow is approximately self-similar (*i.e.* $(gh/U_a^2) \cdot (\partial h/\partial x) \approx 0$ (see Section 2)) the value of $h$ varies proportionally to the downstream distance $x$ measured from the virtual origin and this was given by the expression in equation (2.12). This may be written in the following form:

$$h = C_1(X' + X_0') \tag{4.3}$$

where $X_0'$ is the distance from section A–A (see Fig. 1) to a point upstream from section A–A where the turbulence of the underlying layer is assumed to originate (*i.e.* the virtual origin). Similarly, the variation of the maximum density differences can be written as (see equation (2.12))

$$\frac{\Delta\rho_m}{\rho_a} = C_2(X' + X_0')^{-1}. \tag{4.4}$$

The value of constant $C_1$, $C_2$ and $X_0'$ needs to be determined.

The depth $h$ and the density difference $\Delta\rho_m$ are functions of $X$, $\Delta\rho_0$, $h_0$, $g$ and the velocity ratio $R$, where $\Delta\rho_0$ and $h_0$ are the density difference and the depth of the warm layer at Section A–A respectively. Hence dimensional analysis shows that the dependent variable $h$ and $\Delta\rho_m$ can be expressed in the following form

$$\frac{h}{h_0} = \varphi_1\left(\frac{x}{h_0}, F_0, R\right) \tag{4.5}$$

and

$$\frac{\Delta\rho_m}{\Delta\rho_0} = \varphi_2\left(\frac{x}{h_0}, F_0, R\right). \tag{4.6}$$

In the above equations $\varphi_1$ and $\varphi_2$ denote universal functions of the arguments in the parentheses in which $F_0$ is densimetric Froude number defined later. Since the functions $\varphi_1$ and $\varphi_2$ are not defined specifically, $h_0$ in the above equations can be replaced by the slot width $w$. Thus equations (4.5) and (4.6) can be written in the following forms by considering equations (4.3) and (4.4) *i.e.*

$$\frac{h}{w} = \psi_1(F_0, R)\left(\frac{x}{w} + X_0\right) \tag{4.7}$$

and

$$\frac{\Delta\rho_m}{\Delta\rho_0} = \psi_2(F_0, R)\left(\frac{x}{w} + X_0\right)^{-1} \tag{4.8}$$

in which $\psi_1$ and $\psi_2$ denote universal functions of the arguments in the parentheses, $X_0$ is the non-dimensional distance from point 0 (see Fig. 1) to the point of the virtual origin and $F_0$ is the densimetric Froude number based at the slot and defined as

$$F_0 = \frac{U_0}{\left(g\dfrac{\Delta\rho_0}{\rho_a}w\right)^{\frac{1}{2}}}. \tag{4.9}$$

Universal functions $\psi_1$, $\psi_2$ and $X_0$ are determined from the measured data. The practical purpose of this investigation was to determine the dilution of the warm water (as an effluent) at various sections downstream from the slot. Hence the temperature measurements were carried out in more detail than the velocity measurement (see Section 3). Thus it is reasonable to replace the depth $h$ (characteristic depth) by $\delta$, the depth at which the temperature excess is half of its maximum value (see Fig. 1), if there is a relation between them. It was found experimentally that the relation between $\delta$ and $h$ beyond the zone of recovery can be given as

$$\delta = \lambda h \tag{4.10}$$

where $\lambda$ is a constant about 0.45. The value of $\lambda$ in a wind tunnel experiment with zero pressure gradient for a non-buoyant line source was about 0.64 [11]. Hence with regard to the above result equation (4.7) can be written in the following form

$$\frac{\delta}{w} = \psi_1(F_0, R)\left(\frac{x}{w} + X_0\right). \tag{4.11}$$

The depth $\delta$ was plotted non-dimensionally as shown in Fig. 8. This Figure indicates that the

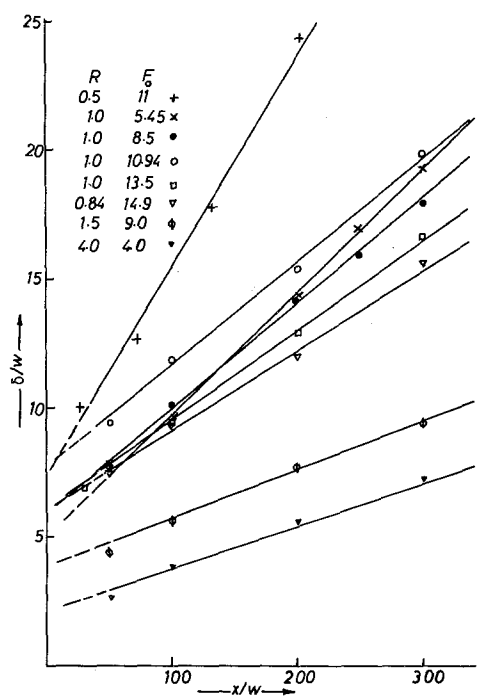


Figure 8. Variation of non-dimensional depth with non-dimensional downstream distance measured from the centre of the slot.

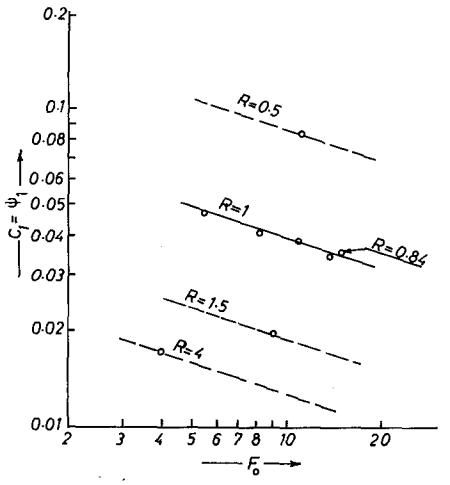


Figure 9. Variation of universal function $\psi_1$ of equation (4.7) with densimetric Froude number $F_0$ and velocity ratio $R$.

non-dimensional depth $\delta/w$ varies linearly with the non-dimensional downstream distance $x/w$ when $x/w$ is greater than 100.

Function $\psi_1$ was calculated from the measured data shown in Fig. 8 by making use of equation (4.11). The results of the calculation are shown in Fig. 9. It can be seen that the calculated points for $R=1$ lie on a reasonably well-defined curve as shown by solid line in Fig. 9. With this information and the lack of further measurements in those cases where the velocity ratio differs from unity, it is assumed that for these values of $R$ a similar variation of function $\psi_1$, as shown by the broken lines in Fig. 9, is a reasonable approach. Figure 9 further shows that the function $\psi_1(F_0, R)$ decreases with the increase of $F_0$ or of the velocity ratio $R$. It was noted that the value of the virtual origin $X_0$ depends largely on the velocity ratio and the outlet Reynolds number $R_e = (U_0 w)/\nu$, where $\nu$ is the kinematic viscosity of the warm water measured at the slot exit. The results of this evaluation are shown in Fig. 10, in which the solid line for $R=1$ is drawn by inspection through the calculated values. In this Figure the assumption is made, based upon the same reasoning given for Fig. 9, that the variation of $X_0$ for the other values of $R$ is the same as that for $R=1$, but that it passes through the corresponding values of $R$ as shown by broken lines in Fig. 10.

It is customary for the type of flow considered here to determine the dilution factor of the

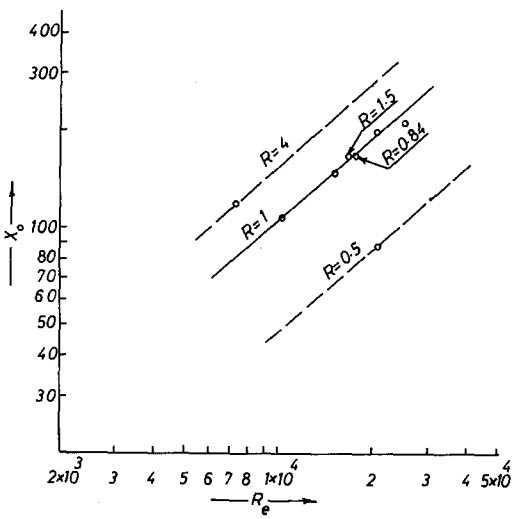


Figure 10. Variation of distance of virtual origin with Reynolds number $R_e$ based on the slot.

underlying flow. This is defined as

$$\frac{\Delta T_0}{\Delta T_m} = \frac{T_0 - T_a}{T_m - T_a}. \tag{4.12}$$

The above expression will be assumed to be the reciprocal of the left-hand side of equation (4.8) when the temperature differences of the fluid causes the buoyancy force, hence equation (4.8) can be written in the following form

$$\frac{T_0 - T_a}{T_m - T_a} = \psi_2'(F_0, R)\left(\frac{x}{w} + X_0\right). \tag{4.13}$$

In equation (4.13) $\psi_2'$ indicates a universal function of the arguments in the parentheses.

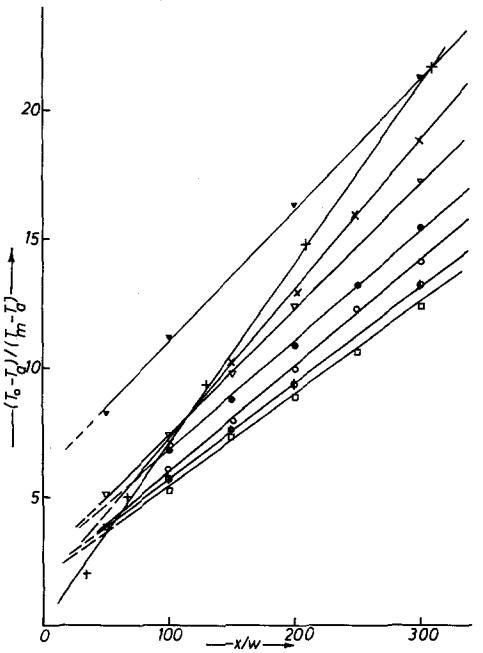


Figure 11. Dilution of the underflowing layer, symbols same as Fig. 8.

The measured values of the dilution factor for various $F_0$ and $R$ are plotted against the non-dimensional downstream distance $x/w$ in Fig. 11, which shows that the dilution factor varies linearly with $x/w$ when $x/w > 100$. This is the region where equation (4.13) is applicable (i.e. beyond the recovery zone). It has previously been pointed out (see footnote in page 10) that the exponent of $x$ obtained experimentally is $-0.9$ which will be $+1.11$ for equation (4.13). This is about unity according to the present experimental results. Fig. 12 shows that the universal function $\psi_2'$ depends on $F_0$ and the velocity ratio $R$. In this Figure the solid line is drawn through the experimental values for $R = 1$ by inspection. Here, as before, due to lack of the experimental results it is assumed that the variation of $\psi_2'$ for the values of $R$ other than unity is similar to that for $R = 1$. Hence in Fig. 12 the broken lines passing through the corresponding value of $R$ are drawn parallel to the solid line. It was also found that the virtual origin varies largely with the Reynolds number $R_e$. This can be seen in Fig. 13. In this Figure it is assumed that the variation of $X_0$ for the value of $R$ differing from one is the same as that defined for $R = 1$. Equation (4.11) and (4.13) were derived under the condition that the flow of the underlying layer is approximately self-similar, *i.e.* that term $(gh/U_a^2) \cdot (\partial h/\partial x) \approx 0$, this means when the utter pressure $p_a$ (see Section 2) does not vary with the downstream distance $x$ from the slot. This, strictly speaking, cannot be true for the flow being considered here unless $U_a$ is large or $\partial h/\partial x$ is very small. This condition may be true for the cases when $R$ is larger than, say 1.5

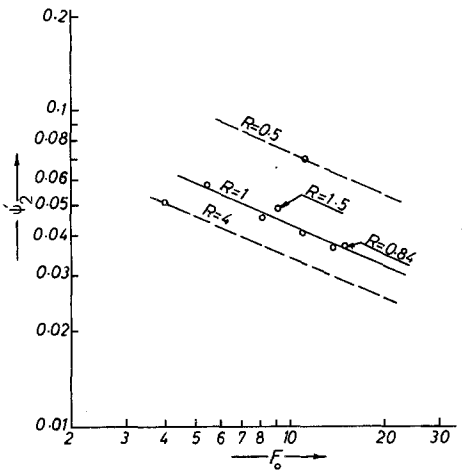


Figure 12. Variation of universal function $\psi_2'$ of equation (4.13) with $F_0$ and $R$.

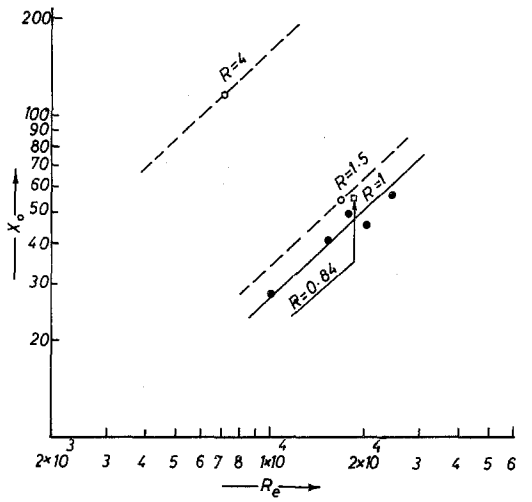


Figure 13. Variation of distance of virtual origin appeared in equation (4.13) with Reynolds number $R_e$.

(see $R=1.5$ and 4 in Fig. 8). The results shown in Fig. 8 indicate that an increase in the ambient velocity $U_a$ causes a decrease in $\partial h/\partial x$ or $\partial\delta/\partial x$ ($h$ is related to $\delta$ see equation (4.10)). Hence it can be concluded that as $U_a$ increases the flow of underflowing layer becomes more and more self-similar. Figures (8) and (11), on the other hand, show that equations (4.11) and (4.13) are valid for the cases when $R<1.5$. This result confirms the statement made in Section 2 that the absence of an analytical similarity does not rule out the existence of an experimental similarity. Figure 9 shows that the values of $\psi_1$ for $R\geqq 1.5$ appear to be close to each other and that they are less close when $R<1.5$. Such a conclusion cannot be made for the results shown in Fig. 12 in which the values of $\psi_2'$ for $R$ above unity are close to each other. Figures 10 and 13 show that the value of $X_0$, defined from the depth of the layer and from the dilution factor, is almost the same when $R=4$, but such a result cannot be obtained for other values of $R$. Although Figs 10 and 13 show that the value of $X_0$ generally increases with the increase of the Reynolds number $R_e$. It may be reasonable to assume that the location of the virtual origin depends on various factors as well as on the physical quantities such as the non-dimensional depth and the dilution factor for the flow in question. It is therefore necessary to determine the value of $X_0$ for equations (4.11) and (4.13) separately. However, the above conclusion should be accepted with reserve and more experimental work is necessary to establish its validity. The coefficient of skin friction expressed by equation (2.18) can now be calculated by making use of equation (4.1) and (4.2) in which the length $\delta$ should be replaced by the characteristic depth $h$ (see equation (4.10)).

Hence the coefficient of skin friction takes the following form

$$\tfrac{1}{2}C_f = C_1\left(\frac{\pi^{\frac{1}{2}}}{2\times 1.85}R_i - 0.07\right) = C_1(0.48\,R_i - 0.07)\,. \tag{4.14}$$

In calculating the above equation the lower limit of the integrals in the bracket of equation (2.18) was taken to be zero, although equation (4.2) may not be applicable for a region very close to the solid boundary. According to Fig. 7 the lower limit $\eta \approx 0.05$ was obtained from a current meter of 1 cm propeller diameter and it is assumed that equation (4.2) can be applied to the region where $\eta$ is less than 0.05. However equation (4.14) shows that the coefficient of skin friction $C_f$ depends on the sectional Richardson number $R_i$, defined by the equation given in expression (2.12) and is a constant for an experimental run. The value of $R_i$ obtained in the experimental runs beyond the recovery zone was ranging between 0.06 and 0.2 and the value of $C_1$ can be obtained from Fig. 9.

**Acknowledgement**

The work described herein was carried out as part of a research programme of the Hydraulics Research Station, and the paper is published by permission of the Director of Hydraulics Research, who also suggested the problem to the writer. The writer wishes also to express his thanks to Mr. J. A. Weller for his help in measurement.

REFERENCES

[1] L. N. Fan, *Turbulent buoyant jets into stratified or flowing ambient fluids*, W. M. Keck Laboratory of Hydr. & Water Resources, California Inst. of Tech., Report No. KH-R-15, (1967).

[2] G. M. Ayoub, *Dispersion of buoyant jets in a flowing ambient fluid*, Ph.D. thesis, Dept. of Civil Eng. Imperial College of Science and Tech. London (1971).

[3] A. R. Agg and A. C. Wakeford, Field studies of jet dilution of sewage at sea outfalls. *J. Inst. of Public Health Eng.*, 71, 2 (1972) 126–149.

[4] N. H. Brooks and R. C. Y. Koh, Discharge of sewage effluent from a line source into a stratified ocean, *I.A.H.R. 11th Int. Congress*, II, (1965) 1–7.

[5] H. O. Anwar, Experiment on an effluent discharging from a slot into stationary or slow moving fluid of greater density, *Journal of Hydr. Research*, 4, (1969) 411–431.

[6] R. A. Sawyer, The flow due to a two-dimensional jet issuing parallel to a flat plate, *Journal of Fluid Mech.*, 9, (1960) 543–560.

[7] R. A. Sawyer, Two-dimensional reattaching jet flows including the effects of curvature on entrainment, *Journal of Fluid Mech.*, 17 (1963) 481–498.

[8] O. G. Sutton, *Atmospheric turbulence*. London, Methuen, 2nd ed., (1955).

[9] G. K. Batchelor, Diffusion from sources in a turbulent boundary layer. *Archiwum Mechaniki Stosowanej*, 3, 16, (1964) 661–670.

[10] J. E. Cermak, Lagrangian similarity hypothesis applied to diffusion in turbulent shear flow, *Journal of Fluid Mech.*, 15 (1963) 49–64.

[11] M. Poreh, *Diffusion from a line source in a turbulent boundary layer*, Ph.D. Dissertation, Colorado State University (1962).